Accepted to Phys. Fluids 10.1063/5.0174014

Coupled Eulerian Wall Film-Discrete Phase model for predicting the respiratory droplets generation during the coughing event

Nguyen Dang Khoa[a)*], Kazuki Kuga (久我一喜)[b)], Kiao Inthavong[c)], Kazuhide Ito (伊藤一秀)[b)]

[a)] Interdisciplinary Graduate School of Engineering Sciences, Kyushu University, Fukuoka, Japan

[b)] Faculty of Engineering Sciences, Kyushu University, Fukuoka, Japan

[c)] School of Engineering, Mechanical and Automotive, RMIT University, Melbourne, Australia

* Corresponding authors

E-mail: ndkhoa@kyudai.jp (NDK)

IGSES, Kyushu University, 6-1, Kasuga-koen, Kasuga, Fukuoka, 816-8580, Japan

Accepted to Phys. Fluids 10.1063/5.0174014

Abstract

Infectious respiratory diseases have long been a serious public health issue, with airborne transmission via close person-to-person contact being the main infection route. Coughing episodes are an eruptive source of virus-laden droplets that increase the infection risk of susceptible individuals. In this study, the droplet generation process during a coughing event was reproduced using the Eulerian wall film (EWF) model, and the absorption/expulsion of droplets was tracked using the discrete phase model (DPM). A realistic numerical model that included the oral cavity with teeth features and the respiratory system from the throat to the first bifurcation was developed. A coughing flow profile simulated the flow patterns of a single coughing episode. The EWF and DPM models were coupled to predict the droplet formation, generation, absorption, and exhalation processes. The results showed that the large droplet number concentration was generated at the beginning of the coughing event, with the peak concentration coinciding with the peak cough rate. Analysis of the droplet site of origin showed that large amounts of droplets were generated in the oral cavity and teeth surface, followed by the caudal region of the respiratory system. The size of the expelled droplets was 0.25–24 μm, with the peak concentration at 4–8 μm. This study significantly contributes to the realm on the site of origin and localized number concentration of droplets after a coughing episode. It can facilitate studies on infection risk assessment, droplet dispersion, and droplet generation mechanisms from other sneezing or phonation activities.

Keywords: Computational Fluid Dynamics, Eulerian Wall Film Model, Discrete Phase Model, Coughing, Droplet site origin and number concentration.

I. INTRODUCTION

Infectious respiratory diseases have long been a significant public health concern. This includes instances of plagues, measles, tuberculosis, influenza, severe acute respiratory syndrome coronavirus (SARS-CoV), Middle East respiratory syndrome coronavirus (MERS-CoV), and the most recent SARS-CoV-2 (Churchyard et al., 2017; Piret & Boivin, 2021). Person-to-person airborne transmission of respiratory viruses can occur via direct or indirect contact, respiratory droplets, and droplet nuclei transmission (Dhand & Li, 2020; C. C. Wang et al., 2021). Infected patients can expel pathogen carriers into the ambient environment via respiratory activities such as breathing, talking, phonating, singing, sneezing, or coughing (Wei & Li, 2016; Stadnytskyi et al., 2021). Once in the surrounding environment, viral-laden droplets can remain airborne for an extended period and transported by indoor airflow to the effective breathing zone of residents, and subsequently inhaled at various exposure levels, as reported by previous studies that were comprehensively reviewed by Inthavong (Inthavong, 2020). During the expiratory phase, the infection risks are associated with the (1) droplet number concentration, (2) size distribution, (3) content of infectious agents, and (4) performance frequency (Morawska, 2006). Besides, more recent studies underscore the dependence of disease transmission on infective dose threshold of the virus (SeyedAlinaghi et al., 2022) and the viral shedding rate (Widders et al., 2020). Thus, quantitative studies are required to determine the pathogen susceptibility targeting each activity.

The threat of coughing-related infections has gained public attention, being extensively studied over the past decades owing to its possibility for the eruptive release of many pathogens in a short period (Stadnytskyi et al., 2021). When coughing, the sequent build-up of expiratory flow velocity, reaching a Reynolds number of 10^4 (Bourouiba et al., 2014), expulses compressed air through the open mouth. Due to the high speed, droplets are produced in the oral cavity due to shear-induced surface-wave instabilities (Wei & Li, 2016; Pöhlker et al., 2021). The stripped droplet parcels follow the air stream and escape to the environment through the open mouth or are re-absorbed into the mucus layer. Virus-laden droplets are generally deposited in the respiratory tract after inhalation (H. Li et al., 2022; C. C. Wang et al., 2021). The mucus clearance process (i.e., coughing) can trigger the re-emittance of deposited virions or the local transmission of progeny viruses shed by infected cells (Schaefer & Lai, 2022). Therefore, the number concentration and size distribution of droplets from coughing have gained significant attention from the scientific community. A review of studies over the past 20 years has indicated significant scatter (Yang et al., 2007; Chao et al., 2009; Morawska et al., 2009; Johnson et al., 2011; Lindsley et al., 2012; Zayas et al., 2012), which can be attributed to the heterogeneity of measurement techniques, sampling methods, or intersubject variability. More recently, facilitated by advanced techniques, the realm of measuring ejected cloud characteristics and generated droplet properties from oral activities in an indoor environment has been embarked upon to deliver a comprehensive understanding during the pandemic epoch

(Wang et al., 2020; Archer et al., 2022; Harrison et al., 2023; Bahramian & Ahmadi, 2023). Drawing upon the properties of generated droplets from experimental studies, computer-aided approaches have been expanded to explore further the deleterious effects of these droplets in the context of disease transmission. Among them, Computational Fluid Dynamics (CFD) has been universally adopted for the numerical investigation of the contagion risk of coughing. Most studies have investigated the cough-jet stream characteristics and fate of expiratory droplets in an enclosed environment (H. Li et al., 2021; Payri et al., 2021; Nie et al., 2022; Aljabair et al., 2023; Nishandar et al., 2023), or the distance-based exposure risks between residents (Calmet et al., 2021; Mariam et al., 2021; Hossain et al., 2023; X. Li et al., 2023). As can be seen, up to date, both experimental and numerical endeavors have extensively advanced our understanding of droplet size distribution and their behavior under varying microclimatic conditions within an enclosed environment. Nonetheless, the site origin and generation mechanism of these droplets in the respiratory tract have yet to be discussed in the listed studies.

Against this background, further numerical studies have been conducted on the interactions between high-speed, chaotic exhaled air and the liquid-layer lining the inner surface of the airway (i.e., the mucus layer) during the coughing episode. The two most common methods adopted are the volume of fluid (Paz et al., 2019; Rajendran & Banerjee, 2019; Pairetti et al., 2021; Yi et al., 2021) and Eulerian wall film (EWF) models (Paz, Suárez, Parga, et al., 2017; Paz, Suárez, & Vence, 2017; Ren et al., 2018, 2020, 2022; Anzai et al., 2022). These studies provide an understanding of the respiratory droplet generation process, the effects of mucus properties on cough clearance efficiency, and the impact of airway deformation. To facilitate the assessment of the infection risks of virus-laden droplets, it is crucial to qualitatively and quantitatively investigate the origin of respiratory droplets during expiratory events (i.e., coughing). Furthermore, the realistic and comprehensive characteristics of the target respiratory airway model should be considered to ensure the accuracy of the cough-jet stream and expelled droplet features.

In this study, the EWF model and Lagrangian discrete phase model (DPM) were coupled to characterize the following: (1) fluid flow profiles of coughing; (2) number concentration, size distribution, and locality of generated and expelled droplet particles during coughing; and (3) absorption efficiency of stripped droplets. The results establish a link between the high viral load of the infected respiratory tract and the possibility of such viral pathogens being released into the environment by coughing. Subsequently, the infection risk can be determined for different respiratory viruses.

II. MATERIALS AND METHODS

A. Numerical model geometry

The realistic airway model comprised a computed tomography (CT)-based trachea-bronchus model and oral cavity produced by the open-source DAZ Studio software (DAZ Productions, Inc.) shown in Fig. 1. During coughing, various oral shapes and sizes were observed (Dbouk & Drikakis, 2020). In this study, the newly developed oral cavity model mimicked the configuration of a slightly open mouth with dimensions of L = 4.7 cm and H = 0.85 cm (Fig. 1) to similarly match the data provided by experimental measurements from high-speed imaging (Dbouk & Drikakis, 2020). The total area of the open mouth of 3.76 cm^2 was within the range of 4 ± 0.95 cm^2, as stated in a previous study (Seminara et al., 2020). In addition, the teeth attributes were integrated to provide the most realistic traits of the oral cavity (Fig. 1). The realistic trachea-bronchus model was created from CT scans, and details on the process are available in the previous study by Ito (Ito, 2016). This trachea-bronchus model, in combination with the nasal cavity, has been validated by our research group, providing reliable results in diverse research themes (C. Wang et al., 2020; Yoo & Ito, 2022; Kuga et al., 2021, 2022, 2023; Murga et al., 2023; Khoa, Li, et al., 2023).

B. Grid design information

The discretization process was executed using the poly-hex core elements, which proposed the CFD simulation with higher accuracy at a reduced computational cost (Zore et al., 2019). The accuracy in the vicinity of the wall was enhanced by applying ten prism layers. This hybrid mesh has been successfully used to predict airflow and particle transportation/deposition simulation of the respiratory tract (Khoa, Phuong, et al., 2023; Khoa, Li, et al., 2023). According to the mesh independence test, the mesh size of 15.5 million cells was selected for subsequent simulation in this study, more detailed information can be found in Fig. S1

(Supplementary Material). This analysis strikes the balance between the computational burden and prediction accuracy.

C. Numerical simulation of airflow pattern

The unsteady, incompressible, and isothermal fluid flow in the human respiratory tract was obtained by solving the Reynolds-averaged Navier–Stokes equations.

$$\frac{\partial \overline{U}_i}{\partial x_i} = 0 \tag{1}$$

$$\frac{\partial \overline{U}_i}{\partial t} + \frac{\partial \overline{U}_i \overline{U}_j}{\partial x_j} = -\frac{1}{\rho_g}\frac{\partial \overline{p_g}}{\partial x_i} + \frac{\partial}{\partial x_j}\left[\left(\nu + \nu_T\right)\left(\frac{\partial \overline{U}_i}{\partial x_j} + \frac{\partial \overline{U}_j}{\partial x_i}\right)\right] \tag{2}$$

where $\overline{U}$ is the mean velocity; u' is the fluctuating components; and p_g, ρ_g, ν, and ν_T are the pressure, density, kinematic viscosity of the fluid, and turbulent viscosity, respectively.

This study selected the turbulent model of the shear stress transport (SST) k-ω . This model has been used to predict adverse pressure gradient flow, strong curvature, and swirling flow in airway systems, as shown in previous experiments (Phuong & Ito, 2015; Elcner et al., 2016). The coughing flow profile was obtained from field measurements of Gupta for male subjects, as shown in Fig. 2A (Gupta et al., 2009). From the empirical equation, the coughing flow rate was allocated to four inlets according to the flow weighting of each lobe of the lung proposed in (Shelley et al., 2014), and reasonably applied in our study (Khoa, Li, et al., 2023), as shown in Fig. 2B. This procedure was implemented via a user-defined function (UDF) macro in ANSYS Fluent. The numerical boundary conditions for the coughing airflow simulation are listed in Table I.

D. Eulerian Wall Film simulation

In a coughing episode, an excessive fluid flow velocity is rapidly produced and subjected to turbulence and high shear stress at the interface between the airstream and thin liquid film (mucus/saliva). Under such conditions, Kelvin–Helmholtz instabilities occur, which cause waves with an escalating amplitude on the surface of a thin liquid film (Pöhlker et al., 2021). Droplets form from the crest of these waves in a multimodal mode and are carried by the flow.

The droplet generation mechanism can be predicted using the EWF model, in which thin liquid mucus layers were hypothesized to be aligned on the inner surface of the oral-tracheal model. The governing equation of the EWF model is as follows (ANSYS, Inc. 2022):

$$\frac{\partial \rho_l h}{\partial t} + \nabla_s \cdot \left(\rho_l h \vec{V}_l \right) = \dot{m}_s \tag{3}$$

$$\frac{\partial \rho_l h \vec{V}_l}{\partial t} + \nabla_s \cdot \left(\rho_l h \vec{V}_l \vec{V}_l + \vec{D}_V \right) = -h \nabla_s P_L + \rho_l h \vec{g}_\tau + \frac{3}{2} \vec{\tau}_{fs} - \frac{3\mu_l}{h} \vec{V}_l + \vec{q}_s \tag{4}$$

$$\vec{D}_V = \frac{\partial}{\partial s} \int_0^h v_l^2 \, dy \tag{5}$$

$$P_L = P_{gas} + P_h + P_\sigma \tag{6}$$

$$P_h = -\rho h \left(\vec{n} . \vec{g} \right) \tag{7}$$

$$P_\sigma = -\sigma \nabla_s . \left(\nabla_s h \right) \tag{8}$$

where ρ_l is the film density, h is the film height, V_l is the mean film velocity, and m_s is the mass source per unit wall area owing to droplet collection, film separation, film stripping, and phase change. In Equation 4, D_V is the differential advection term computed based on the quadratic film velocity with fluctuating velocity $v_l(s,y,t)$, in which s is the horizontal flow direction and y is the vertical direction (Kakimpa et al., 2015). The term P_L is the mucus film pressure, g_τ is the gravity component, τ_{fs} is the shear force at the film–liquid interface, μ_l is the viscosity, q_s is the momentum source, σ is the surface tension, P_σ is the pressure exerted by the surface tension, P_h is the gravity component normal to the wall, and n is the normal vector.

The reliability of applying the EWF model in anticipating the interaction between the coughing stream jet and lining fluid is emphasized through supplementary simulations conducted using a simplified airway model. The simulation results were subsequently compared with experimental data, and additional information on this validation process is elaborated upon in Fig. S2 (Supplementary Material).

In the context of our primary simulation, the EWF model was included with the fluid flow at the beginning of the coughing episode. The simulation was applied to the total inner surface of the numerical domain, including the teeth surface. In general, the mucus thickness varies along the airway system. However, to simplify the simulation, a constant thickness of 30 μm was used to represent the mucus layer in the throat, larynx, trachea, and bifurcation, based on previous studies (Paz, Suárez, Parga, et al., 2017; Paz, Suárez, & Vence, 2017; Ren et al., 2022; Anzai et al., 2022). For the oral cavity, the saliva thickness ranged from 11.3 to 68.9 μm, as proposed by the research of Assy (Assy et al., 2022). For the teeth surface, the saliva thickness was assigned based on early experimental data (Collins & Dawes, 1987), which ranged from 2.59 to 4.44 μm following the mandibular, maxillary, left, or right position of teeth. The saliva and mucus layers were assumed to be water with a density of 998.2 kg/m^3 and viscosity of 0.001 kg/m s.

Shear-induced droplet generation was considered through the high velocity and turbulent flow, causing the instability of the lining mucus/saliva layers and leading to droplets peeling from the crests of the formed waves. This process was defined by the initial parameters given in Table II. Among them, the critical shear stress is the main factor that governs the number concentration of generated droplets. A parametric analysis was required prior to the main simulation to determine an appropriate value for the simulation, which is delivered in Fig. S3 (Supplementary Material). Notably, this analysis was significantly influenced by the individual morphological characteristics considered in this study. Then, a value of 5 Pa was specified for the critical shear stress, which imposed the limit that any region subjected to shear stress greater than 5 Pa would trigger the shedding of mucus/saliva layers into droplets. In addition, a diameter coefficient, which specifies the droplet size range (ANSYS, Inc. 2022), was also determined by experiencing the parametric analysis with a value of 0.0003 (Fig. S4, Supplementary Material). Finally, the film time-step size was automatically assigned by ANSYS Fluent using adaptive time-stepping functions, which controlled the time-step size to be small enough to ensure that the maximum Courant number during the simulation was less than 1. The continuous generation of mucus/saliva layers beneath the epithelial cells was neglected, which indicated no refill of mucus/saliva layers after being dispossessed.

E. Discrete Phase model simulation

The EWF model was coupled with the DPM to track the trajectories of droplets stripped from the liquid film. Forces acting on the body were used to predict the droplet transportation, absorption, and exhalation characteristics of the oral-tracheal model. The Lagrangian discrete phase of the particle trajectories was computed by Equation 9.

$$\frac{d\vec{u}_p}{dt} = \vec{F}_D + \vec{F}_G + \vec{F}_S \tag{9}$$

where the subscript p is the droplet phase and $\vec{F}_D$ is the drag force per unit particle mass derived from Stokes' drag law, expressed in Equation 10.

$$\vec{F}_D = \frac{18\mu}{\rho_p d_a^2}\frac{C_D \mathrm{Re}_p}{24}\left(\vec{U} - \vec{u}_p\right) \tag{10}$$

where μ is the air viscosity, $\vec{U}$ is the fluid flow velocity, $\vec{u}_p$ is the droplet velocity, d_a is the aerodynamic droplet diameter, ρ_p is the droplet density, C_D is the drag coefficient, and Re_p is the particle Reynolds number.

The second term, $\vec{F}_G$, denotes the gravitational settling. The third term, $\vec{F}_s$, is Saffman's lift force due to shear on a unit mass basis. The lift force was adapted from a previous study by Li and Ahmadi (A. Li & Ahmadi, 1992), and is a generalization of the expression provided by Saffman (Saffman, 1965), expressed as Equation 11.

$$\vec{F}_S = \frac{5.188 v^{1/2} \rho d_{ij}}{\rho_p d_a \left(d_{lk} d_{kl}\right)^{1/4}} \left(\vec{U} - \vec{u}_p\right) \tag{11}$$

where d_{ij}, d_{lk}, and d_{kl} are deformation rate tensors.

The aerodynamic diameter and number of tracked droplets were determined based on the EWF simulation. The droplets were defined with a unit density (1000 kg/m^3), equal to that of pure water. The fate of the droplets was considered as exhaled via the mouth opening or was re-absorbed into the mucus layer; hence, the "escape" boundary condition was assigned to the mouth opening, and the "perfect trap" condition was applied as the wall boundary conditions. The evaporation and breakup of the droplets were negligible. The droplets were continuously generated during the simulation; therefore, the velocity, size, and spatial and temporal information of the droplets stripped from the mucus layer were recorded using the UDF macro for each time-step.

The generated, exhaled, and absorbed percentages, denoted as η_{G-i}, η_{E-i}, and η_{A-i}, can be expressed by Equations 12, 13, and 14, respectively.

$$\eta_{G-i} = \frac{N_{G-i}}{N_G} \times 100\% \tag{12}$$

$$\eta_{E-i} = \frac{N_{E-i}}{N_E} \times 100\% \tag{13}$$

$$\eta_{A-i} = \frac{N_{A-i}}{N_A} \times 100\% \tag{14}$$

where N_{G-i}, N_{A-i}, and N_{E-i} are the number of droplets generated, absorbed, and exhaled that belong to region i, which corresponds to the regions defined in Fig. 1. N_G, N_A, and N_E are the total stripped, absorbed, and exhaled droplets after a single coughing episode (duration of 0.5

s), respectively. The size distribution of the coughed droplets was multimodal; accordingly, the droplet size bin was identified to establish the size distribution percentage of the generated, exhaled, and absorbed droplets ($\eta_{G\text{-}s}$, $\eta_{E\text{-}s}$, and $\eta_{A\text{-}s}$), given in Equations 15, 16, and 17, respectively.

$$\eta_{G-s} = \frac{N_{G-s}}{N_G} \times 100\% \tag{15}$$

$$\eta_{E-s} = \frac{N_{E-s}}{N_E} \times 100\% \tag{16}$$

$$\eta_{A-s} = \frac{N_{A-s}}{N_A} \times 100\% \tag{17}$$

where $N_{G\text{-}s}$, $N_{A\text{-}s}$, and $N_{E\text{-}s}$ are the number of droplets generated, absorbed, and exhaled, respectively, which decreases in the size bin, as listed in Table III.

The size distribution of exhaled droplets can be calculated by dividing the number of droplets within the specific size bin by the logarithm of the droplet size class interval ($dN_{E\text{-}s}/dLogD$). Finally, the exhaled droplet size distribution was normalized with the total cough exhaled volume (1,000 cm^3) to obtain the number concentration divided by the logarithm of the droplet size class interval ($dC_{NE\text{-}s}/dLogD$).

III. RESULTS

A. Coughing fluid flow characteristics

The results of the coughing fluid flow features are depicted in Fig. 3 at the start of the coughing episode at 0.01 s, cough peak flow rate (CPFR) at 0.077 s, and near the end of the coughing event at 0.4 s. Notably, the velocity magnitude and distribution herein are described at the instantaneous times. At the onset of coughing (Fig. 3A), the culminated velocity occurred at the bifurcation, trachea, glottis, and throat regions with a value of 3 m/s. At CPFR, the spatial distribution of the jet stream remained, but the magnitude increased by almost 13-fold up to 40 m/s. In the final coughing stage, the coughing velocity rapidly decreased to less than 3 m/s in identical acceleration regions.

In the oral cavity (Fig. 3B), the airstream accelerated in the throat region and impacted the palate and bends following the curvilinear shape of the oral ceiling. The expulsive flow that escaped the oral region was primarily distributed at the bottom of the mouth opening. Reserve flow also formed in the basal region near the mouth opening, which contributed to the swirling flow at the mouth opening (Fig. 3B). Due to the flow features toward the ceiling of the oral cavity, the maxillary teeth are expected to endure the high-velocity flow during the cough. Fig. 3C shows the two-dimensional flow distribution for the maxillary teeth, which revealed that the high-velocity fluid flow attacked the inner surface of the molars, premolars, canines, and incisors.

B. Droplet generation mechanism during coughing

The rapid increase in the flow rate due to coughing induces substantial shear stress on the airway wall, closely linked to the droplet production criteria in the EWF model simulation. The relationship between shear stress, mucus thickness, and stripped droplets is presented in Fig. 4, which describes the instantaneous value of each variable. At 0.01 s (Fig. 4A), the low coughing

Accepted to Phys. Fluids 10.1063/5.0174014

velocity resulted in a modest shear stress of less than 5 Pa on the airway wall, which failed to meet the minimum threshold to produce droplets; hence, the droplets were not observed and the mucus/saliva thickness remained in its original state. At CPFR (Fig. 4B), the cough ejection velocity increased to 40 m/s, which induced significant shear stress on the wall surfaces. Multiple airway surfaces experienced shear stress levels greater than 5 Pa, which fulfilled the criterion for droplet generation off the thin liquid film on the oral-airway surfaces. Accordingly, the mucus/saliva thickness decreased to almost 0 μm and droplets simultaneously emerged in the corresponding regions (Fig. 4B). The complex and uneven surface of the oral-airway model produced an uneven distribution of the peak shear stresses. This completely removed the mucus/saliva layers in several specific regions while the remaining areas preserved their initial liquid film thickness. Droplet production decreased significantly at 0.15 s (Fig. 5C) due to the mucus/saliva layers dissipating, following the former intense erosion process during CPFR.

C. Properties of generated droplets during coughing

The relationship between the coughing flow profile and droplet production was correlated to understand the droplet generation process better. The instantaneous number of droplets stripped from the mucus/saliva layers due to the coughing flow rate during the single coughing episode (~0.5 s) is shown in Fig. 5A. The results demonstrate that the coughing flow rate rapidly increased in the early stage of coughing. In contrast, droplet generation lagged and didn't start until 0.04 s with an initial rapid rise. The number of droplets produced increased rapidly in parallel with the coughing flow rate and formed a sharp slope, with the peak almost coinciding with the CPFR (at approximately 0.077 s). After reaching their peaks, the cough flow rate and number of stripped droplets exhibited a downward trend. The number of droplets produced rapidly dropped to almost 0 at 0.25 s, in contrast to the cough flow that gradually decreased to 0 taking 0.5 s. After the single coughing episode, 11,594,566 droplets were generated (Table IV). The instantaneous position of the droplets during different times during the cough are shown in Fig. 5B for time, t = 0.025, 0.04, 0.077, and 0.2 s, where the droplets are colored by diameter. The results indicate an early appearance of droplets in the bifurcation and throat regions (at 0.025 s). At 0.04 s, a dense population of droplets was observed in the bifurcation and oral cavity, which corresponds to the airway curvature of the palate region in line with the flow distribution in the oral cavity. At CPFR at t = 0.077 s, the oral-airway model is filled with a very high density of droplets due to the rapid droplet production (shown in Fig. 5A). At t = 0.2 s, most of the droplets were re-absorbed into the mucus/saliva layers or transported by the coughing flow toward the oral region and released into the external environment via the mouth opening. Hence, fewer droplets are found in the airway compared to the oral cavity. Furthermore, the droplet size was less than 10 μm for the entire coughing episode.

One advantage of this study is that it provides details on the origin of the stripped droplet during the coughing event, illustrated in Fig. 5C. The oral region was identified as the primary source of droplets (up to 46.8%) during the cough. In the remaining regions, the droplet production levels were similar (approximately 11.9–14.3%), slightly reducing towards the bifurcation region. The large amount of stripped droplets in the oral cavity is attributed to higher shear stresses (exceeding 5 Pa) than in other regions. Fig. 5D shows the total surface area (cm^2) of each region subjected to shear stress of >5 Pa, where the oral cavity exhibited the highest surface area. Therefore, more droplets were produced from the saliva film in the oral airway region.

The percentage of droplets generated per droplet diameter size bin can be estimated using Equation 15, as shown in Table IV. Most droplets produced were in the size interval of 4–8 μm (approximately 78.01%), followed by 2–4 and 8–16 μm, respectively. The droplets in the size bin of <1 μm had a low percentage of 0.078–0.181%, while for the larger size bins (>16 μm), the rate was only 0.169%.

D. Properties of exhaled droplets during coughing

An analysis of the expelled droplet concentration for different droplet diameters was performed and compared with experimental measurements of Yang (Yang et al., 2007). In the experimental work, 54 volunteers of varying ages and genders coughed into a sampling bag with a well-controlled relative humidity; thus, the coughed droplets retained their original size. Fig. 6A shows the number concentration of droplets at the mouth opening plotted against the average droplet size and compared with Yang (Yang et al., 2007). The EWF model closely matched the profile with the measured exhaled number concentration. There was a sharp increase in the number concentration for droplet sizes approximately at 2 μm before reaching a peak concentration (approximately 2,500/cm^3) at 4–8 μm. After the peak, a downward trend was observed, and the cutoff diameter where no droplets were expelled was >10 μm.

The source of droplets expelled to the environment is shown in Fig. 6B, where the oral cavity (including the teeth surface) was responsible for the largest amount of droplets exhaled into the environment (up to 75%). The amount gradually reduced for the geometry moving posteriorly toward the caudal airway; specifically, 12.3% originated from the throat, followed by the larynx (approximately 8.3%), trachea, and bifurcation (approximately 2.2%), respectively.

Most exhaled droplets, 73.1%, were between 4-8 μm due to the highest percentage of droplets produced in this range (Table IV). For smaller droplets, the exhalation rates were 12.8% and 8.9% for size bins of 2–4 μm and 8–16 μm, respectively. Despite the low production rate of droplets in the size bin of <1 μm, the appearance of these small droplets in the exhaled breath was 0.49–0.79%.

The spatial distribution of the droplets that escaped through the mouth during the coughing is illustrated in Fig. 6C, where the different droplet colors denote the source location. The results show that the oral cavity is the primary location of the expelled droplets, and the droplets exit through the entire space of the mouth opening. For the other airway regions (throat, larynx, trachea, and bifurcation), the expelled droplets mainly dispersed through the lower half of the mouth opening. There was a small scattering of droplets in the upper half of the mouth opening. Despite the significant variation in the vertical distribution of droplets expelled, the horizontal distribution in the lower half was consistent. This distribution was due to the oral cavity shape and the exhaled jet stream found in the lower half of the mouth opening (shown in Fig. 3).

E. Absorbed efficiency of droplets during coughing

The total number of droplets absorbed onto the mucus/saliva layers was 10,128,559 (Table IV), accounting for approximately 87.3% of the total droplets produced by the cough. The primary absorption region was the oral cavity (including the teeth surface), with 47.8%. In contrast, in the remaining regions, the absorption efficiency significantly decreased by approximately four-fold in the 11.2–14.1% range. Most of the generated droplets re-absorbed into the oral region's saliva layer can be associated with the complex morphology of this region, which prevented the smooth movement of the droplets.

Fig. 7B shows the droplet absorption efficiency categorized by the region where the droplets originated from (e.g. slice color indicates the droplet source location). In general, droplets were immediately re-absorbed back into its own region where they were generated. For example, 87.5% of droplets produced in the oral cavity re-absorbed in its region, and that of the throat, larynx, trachea, and bifurcation, the re-absorption rate was 88.2%, 91.9%, 93.1%, and 100%, respectively.

The cough-jet stream began from the tracheal bifurcation, and the oral region had the greatest exposure to all droplets originating from lower regions, including the throat (5.3%), larynx (4.2%), trachea (1.8%), and bifurcation (1.3%). This geometry and flow feature explains the lack of absorbed droplets from geometrically lower regions (e.g. upstream flow) than the region itself since the jet flow transports the droplets from the bifurcation to the oral cavity. Droplets with sizes of 4–8 μm (Table IV) were the most re-absorbed due to the greater number of generated droplets in this size bin. For the other size bins, the absorption rate was similar to its generation rate.

Fig. 8 shows the deposition pattern on specific airway regions based on where the droplets were produced. Deposition in the oral cavity showed that the focal absorption region occurred in the palate regardless of the droplet origin. Most droplets in the throat tended to accumulate in the upper and branching regions. In the larynx and trachea, there was a high rate of re-absorption from itself. Only the droplets produced by itself were re-absorbed for the bifurcation, and most were observed in the left bifurcation.

Generally, the cough-jet stream influenced droplet deposition in the oral airway, and the droplet absorption patterns coincided with the high-velocity regions, as discussed in the previous section.

F. Role of teeth surface in the simulation of droplet generation during coughing

The results reveal the critical role of the oral cavity in droplet generation, emission, and absorption. This raises the question of the contribution of the teeth surface to the areas of interest in this study. In this section, the droplet generation, absorption and exhalation from the oral cavity were divided into the teeth surface and the remaining portion of the oral airway surface (shown in Fig. 9A). The total of 46.8% of droplets that were produced from the oral cavity (from Fig. 5C), were found to originate evenly between the teeth surface and remaining portion (approximately 23%).

The instantaneous shear stress at 0.04 s and 0.077 s is given in Fig. 10A. Shear stress >5 Pa was observed on the maxillary incisor surface in the early stage of the coughing event (0.04 s). A high shear rate was found on the inner surface of the maxillary teeth, including the incisors, canines, and molars, at the CPFR (0.077 s). Consequently, many droplets were stripped from the saliva layers along the inner side of the maxillary teeth surface (Fig. 10B). This phenomenon is closely associated with the cough-jet stream, which impacted the upper jaw, as discussed in the previous section.

For the expelled droplets (Fig. 9B), approximately 40% was derived from the teeth's surface. This was attributed to the droplets that formed on the teeth surface, especially on the incisors, which travelled a short distance without any obstacles to the mouth opening. For the re-absorption capacity, the larger surface area of the remaining portion of the oral region caused a larger number of droplets to re-absorb (approximately 27%). In comparison, 21% of droplets re-absorbed onto the teeth surface.

Figure 11 presents both the quantitative analysis and spatial distribution of droplets absorbed on the teeth surface. Primarily, the quantitative analysis serves to delineate the proportion of total absorbed droplets on the teeth surface, which was generated from distinct regions within the model. The findings revealed that out of the total number of droplets absorbed on the teeth surface, 81.02% of absorbed droplets originated from this area. Subsequently, droplets emanating from the oral cavity constituted 14.79% of the total absorbed droplets on the teeth surface. The percentage gradually reduced for the posterior regions and reached 0.45% for the bifurcation, which implies a limited quantity of droplets stemmed from this region absorbed onto the teeth surface. In addition, the spatial distribution of the droplet deposition on the teeth surface indicates that most droplets tended to settle on the inner surface of the maxillary teeth or partially in the mandibular molars and canines, regardless of their origin.

IV. DISCUSSIONS

The coupled EWF-DPM model was applied to explore droplet generation and flow behavior during a single coughing event, where the origin and local number concentration of the generated, absorbed, and expelled droplets were determined. This study first analysed the coughing flow rate, which provides insight into the droplet generation process during coughing. The rapid development of airflow velocity along the airway and oral cavity subjected the surface walls to high shear stress, which caused the stripping of mucus/saliva layers into droplets. The airstream accelerated through the narrow airway lumen (e.g., trachea, glottis, and throat regions), consistent with a previous study (Kou et al., 2018). Thus, the predicted fluid flow is recognized as a constant feature of coughing in terms of the velocity distribution but would vary in magnitude depending on the lumen diameter of individual airway structures. In the oral cavity, this study included the teeth geometry, which has been lacking in reported simulation studies of the fluid flow characteristics during coughing. Our results indicate a strong interaction between the cough-jet stream and maxillary teeth surface, which could influence droplet generation and absorption/exhalation.

The shear-induced droplet generation due to the high-speed velocity is one of the four generation mechanisms that mainly occurs in the main bronchus, trachea, and larynx regions (Pöhlker et al., 2021). The results revealed an essential connection between the shear stress and the number concentration of generated droplets, summarized as follows. The higher the coughing flow rate, the greater the shear stress, and the larger the number of droplets generated. This relationship indicates the uncertainty of the generated droplet number concentration owing to the coughing flow profile, particularly at the CPFR. For instance, the significant diversity between individuals and genders has been recorded for coughing parameters, such as the peak velocity, peak velocity time, and coughing duration by field measurements (Han et al., 2021). These variations are expected to affect droplet generation. In addition, the fidelity of the numerical domain needs to be considered. Earlier simulation studies used an idealized model that proposed a smooth shear stress distribution on the wall surface (Anzai et al., 2022). The study by Ren et al. (Ren et al., 2022) reported a nonuniform distribution of shear stress on a realistic lower airway wall. The results showed heterogeneities in spatial distribution and magnitude of shear stress compared with ours; consequently, the droplet generation differed. Nevertheless, the coughing flow profile, realistic attributes, and intersubject variability presented challenges, and the simulation results need to be benchmarked against the experimental results.

For infection risk assessment, it is crucial to understand the origins of droplets during expiratory activities within a specific area and to quantify the droplets generated from each source (Morawska, 2006). For coughing, droplet-released sources are well established and consist of the lungs, trachea, nasopharynx-larynx, and nasal and oral passages (Stadnytskyi et al., 2021; Zhou & Zou, 2021). However, the exact location of droplet generation/exhalation and their localized number concentration remain uncertain. Our droplet generation analysis indicates that the most likely sources of droplets produced during coughing were the oral cavity and teeth surface. Although common respiratory viruses primarily occur in the epithelial cells of the respiratory system (Alexander-Brett & Holtzman, 2015), evidence suggests high viral loads of SARS-CoV-2 in saliva samples from an asymptomatic cohort and the active replication of infected cells in the oral cavity (Huang et al., 2021). In addition, previous clinical studies have detected SARS-CoV-2 in patient saliva (To et al., 2020; Wölfel et al., 2020; Wyllie et al., 2020). Thus, from our results, the high infection risk of SARS-CoV-2 may be associated with a high droplet concentration in the oral cavity. Apart from the oral cavity, the deposition site can be determined in the airway system of the potential host (C. C. Wang et al., 2021), but this depends on the aerosols or virus-laden droplet size. Droplets from the deposition regions may cause the re-emission of progeny viruses shed by infected cells (Schaefer & Lai, 2022). Therefore, the possibility of transmission droplets originating from the respiratory system was indicated by our analytical data, where considerable quantities of exhaled droplets were recorded from the throat, larynx, trachea, and bifurcation. The results showed that the generation sites of droplets tended to be in a particular position rather than evenly distributed.

The site of origin affected the potential direction of the droplet cloud during a cough. Our results showed that exhaled droplets from the oral cavity escaped to the surroundings at all locations and angles from the mouth opening; hence, the droplets travelled further and dispersed widely. Meanwhile, exhaled droplets stripped from the respiratory airway exhibited a downward direction as they exited the mouth into the ambient environment. This phenomenon is expected to direct the droplets to the ground outside. Thus, our location-specific results can inform studies on the threat of coughing-related infections in indoor environments.

In addition to identifying the origin site, the local number concentration and size distribution of droplets exhaled during coughing were determined. Based on the literature review, these two parameters were estimated for a varied population and measurement techniques. As summarized in Fig. S5 (Supplemental Material), the field measurement data were scattered broadly regarding the size distribution and number concentration. In particular, the peak number concentration was recorded in the 4–8 μm range proposed by Yang and Chao (Yang et al., 2007; Chao et al., 2009). This peak shifted to 0.75–2 μm in the experiment by Morawska and Johnson (Morawska et al., 2009; Johnson et al., 2011). The highest number concentration was recorded at a much smaller size, at 0.3 μm measured by Lindsley and Zayas (Lindsley et al., 2012; Zayas et al., 2012). In addition, the number concentration among the references indicated significant variations. Therefore, our analysis was validated by recruiting one specific experimental data from Yang et al (2007). Both experimental and simulated data showed that a 4–8 μm droplet size was formed and exhaled at a high number concentration during coughing. Within this size range, the expelled droplets would travel further into the environment and suspend for longer, enhancing the exposure risk of residents in a confined space (Jones & Brosseau, 2015; Dhand & Li, 2020; Bourouiba, 2021). Nevertheless, the lifetime and size of droplets have a complex relationship with many environmental factors, including temperature, humidity, and ventilation mechanisms (Jayaweera et al., 2020; Bahramian, 2023). Once inhaled by a susceptible person, fine aerosols (<5 μm) have a high possibility of escaping the defence mechanism of the upper airway and penetrating the lower airway, which is often associated with higher severity, morbidity, and fatality (Zuo et al., 2020; Sosnowski, 2021). A more significant amount of viral genomes of common respiratory viruses have been revealed in fine aerosols (<5 μm) compared with larger ones (Gralton et al., 2013; Yan et al., 2018). Information regarding the site origin and local number concentration was revealed by our analysis, which may not be possible in field measurements with volunteers owing to ethical and technical barriers.

Our simulation data showed that one issue that should be addressed in droplet generation, absorption, and exhalation studies is the inclusion of detailed oral cavity and teeth features. The oral cavity was a significant source of droplet expulsion; however, due to its complex anatomy with the existence of the teeth, the region provided a source for droplet absorption, thereby contributing to the mitigation of droplet emissions from caudal respiratory areas. By eliminating realistic features or simplifying the oral cavity, the high local concentrated absorption regions may shift to the larynx-throat region, according to our data and a previous simulation (Guo et al., 2020), allowing more droplets to be expelled. Thus, the realistic anatomy of the oral cavity alters the number concentration and spread angle of ejected droplets, thereby changing the dispersion and migration characteristics of the expelled droplets.

Throughout the discussion points, it is noteworthy that the data was obtained upon the assumption of one single cough event. Concerns may arise regarding whether introducing a successive coughing process would impact the results. In this context, the previous experimental research revealed the second cough characteristics with a homogeneous profile but weakened mechanical effectiveness, such as cough peak flow rate and expired volume

(Gupta et al., 2009; Hegland et al., 2013). This weakening was prolonged until the end of the cough epoch. Upon these conditions, outcome variation can be anticipated as following points:

(i) Within the coughing flow patterns, continuous accelerations are expected to occur during each coughing episode, with the highest magnitude in the first cough and a precipitous decline in the subsequent cough events.

(ii) Regarding the generated droplet number concentration, although a number concentration increase is conceivable, it would not anticipated to yield a significant deviation from the current results. This expectation is rooted in the observation that the mucous membrane almost diminished after the initial coughing event, as indicated in Fig.4. Additionally, the WSS exerted on the respiratory wall may fall below the given CSS and be insufficient to trigger the droplet stripping.

(iii) In terms of droplet behaviors (absorbed or expelled), consecutive acceleration of fluid flow can result in the variation of the absorption rate due to the inertia, subsequently leading to the corresponding alternations in the escaped rate.

Henceforth, subjecting the current research to successive cough simulations while maintaining consistent initial conditions is expected to yield modest variations. Hence, it may be reasoned that the applicability of the results may be regarded as akin to the current findings under the assumption of a single cough process.

V. CONCLUSIONS

Detailed information on the droplet generation, exhalation, and absorption behavior in a realistic oral-tracheal model was elucidated using the coupled EWF-DPM model. The main points of the analysis are summarised as follows:

- The EWF model reliably predicted the interaction between the free stream and liquid film lining by validating it against measured data. Coupled with the DPM model, the concentration profile of exhaled droplets from the mouth opening after a coughing episode could represent experimental data.
- The morphometry fidelity of the oral-tracheal model and the coughing flow rate affects the cough-jet stream and is expected to alter droplet generation, transportation/absorption, and exhalation.
- Shear stress at the liquid film-air interface is a critical factor governing the droplet generation properties. Therefore, appropriate values as the input criteria for the EWF and benchmarking against experimental data are required.
- The oral and teeth surface were primary locations for droplet generation. While other regions of the respiratory system showed a much lower droplet production rate. The rates gradually decreased toward the posterior regions.
- Most exhaled droplets were 4–8 μm in diameter. Droplet sizes of <1 μm and >10 μm were also detected but were much fewer upon exhalation through the mouth opening.

- Including the teeth surface provided a more realistic simulation, directly influencing the droplet number concentration that could be expelled through the mouth opening.

Our simulation can be a foundation for further studies on droplet cloud generation and the transmission of viral genomes in the environment from sneezing, speaking, singing, or phonation activities. It also provides quantitative and qualitative assessments of infection risk based on the site of origin, size distribution, and localised number concentration.

VI. FIGURES

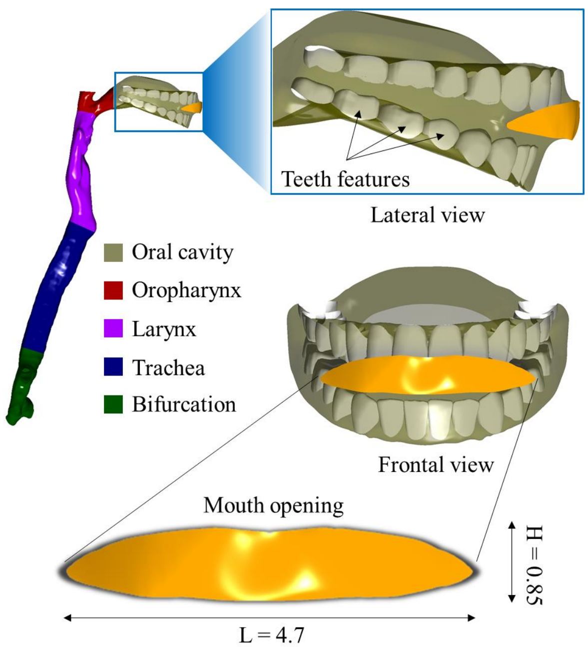

FIG. 1. Outline of the simulation model

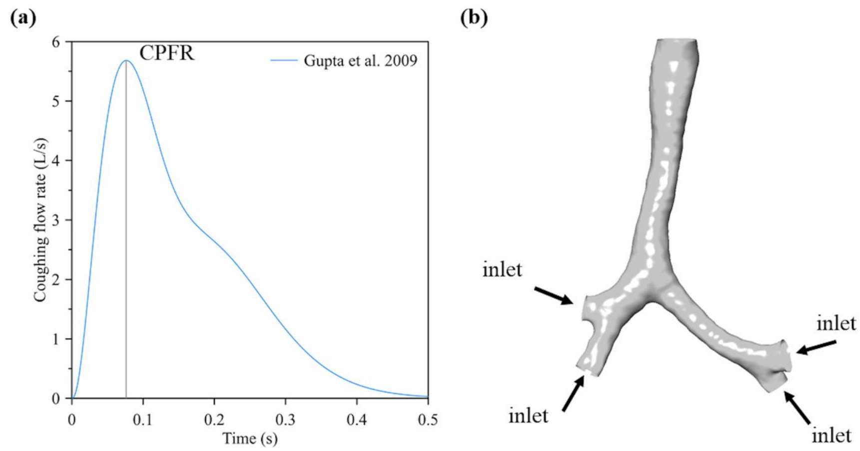

FIG. 2. (a) Coughing flow rate following the previous field measurement. (b) The description of inlet boundary conditions.

Accepted to Phys. Fluids 10.1063/5.0174014

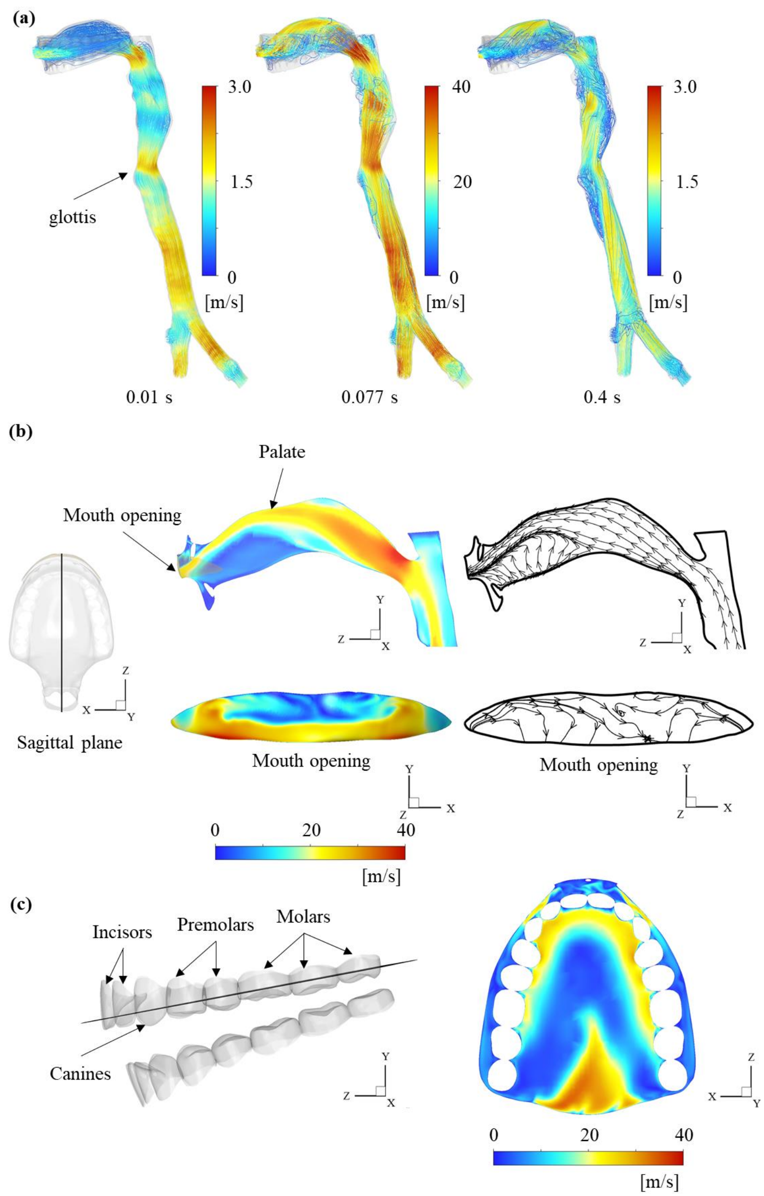

FIG. 3. (a) Instantaneous streamline velocity distribution at the specific time during coughing. (b) Instantaneous 2D flow features in the oral cavity and the mouth opening, and (c) in the vicinity of the maxillary teeth surface at the CPFR (0.077 s)

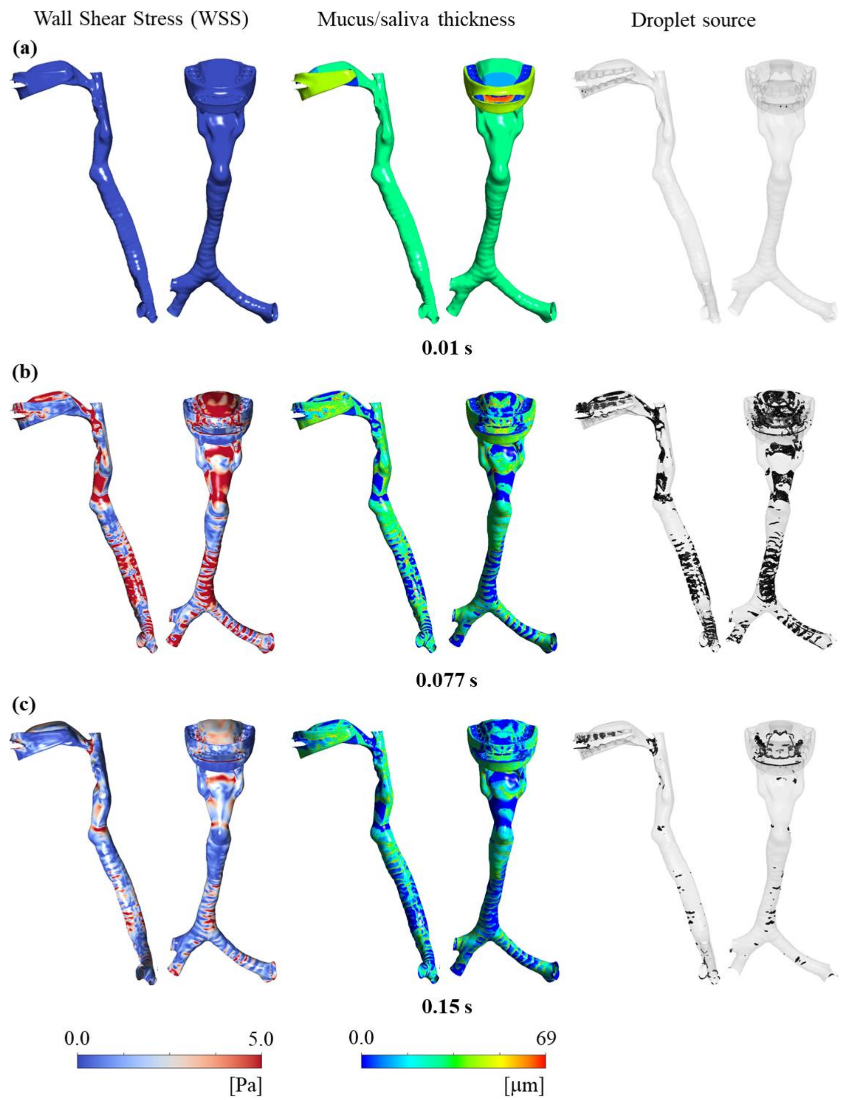

FIG. 4. The immediate distribution of wall shear stress (left), mucus/saliva thickness (middle), and initial position of stripped droplets (right) at (a) 0.01 s, (b) 0.077 s, and (c) 0.15 s.

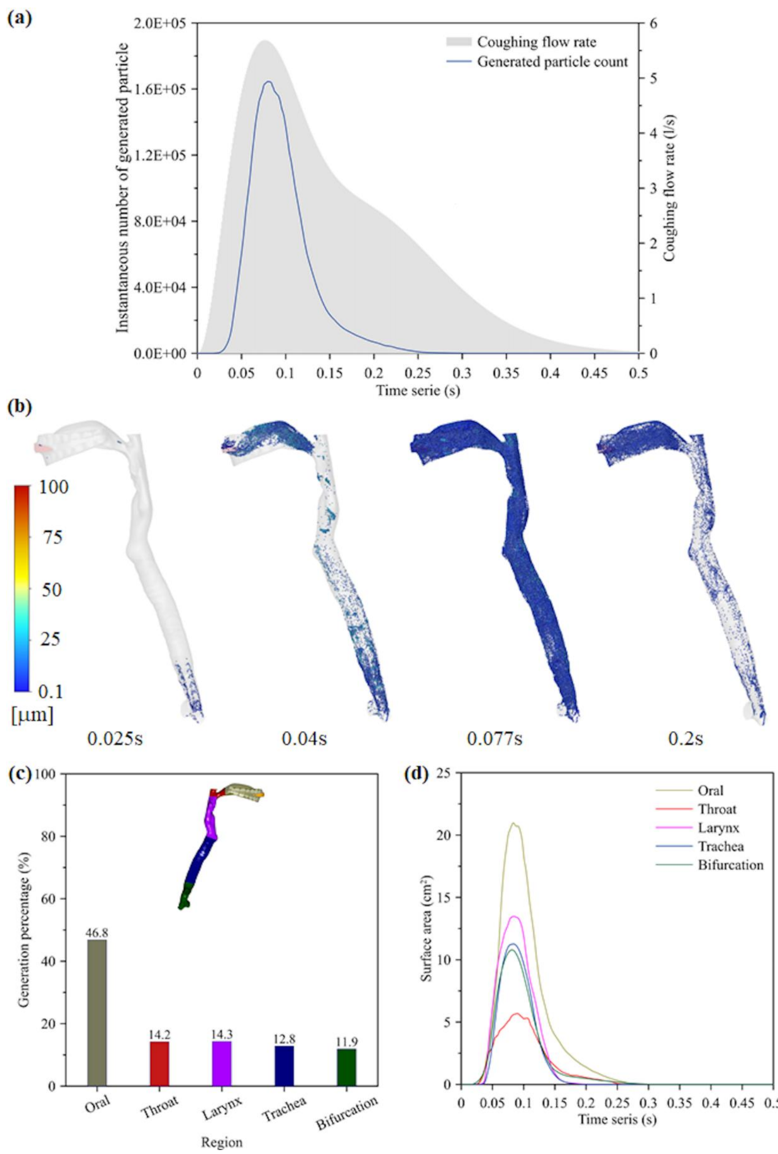

FIG. 5. (a) The instantaneous number of generated droplets during the cough event associated with the coughing flow rate. (b) Instantaneous positions of droplets at different times during the cough. (c) The percentage of droplets produced from their origin. (d) The surface area of each airway region that experienced wall shear stresses greater than 5 Pa.

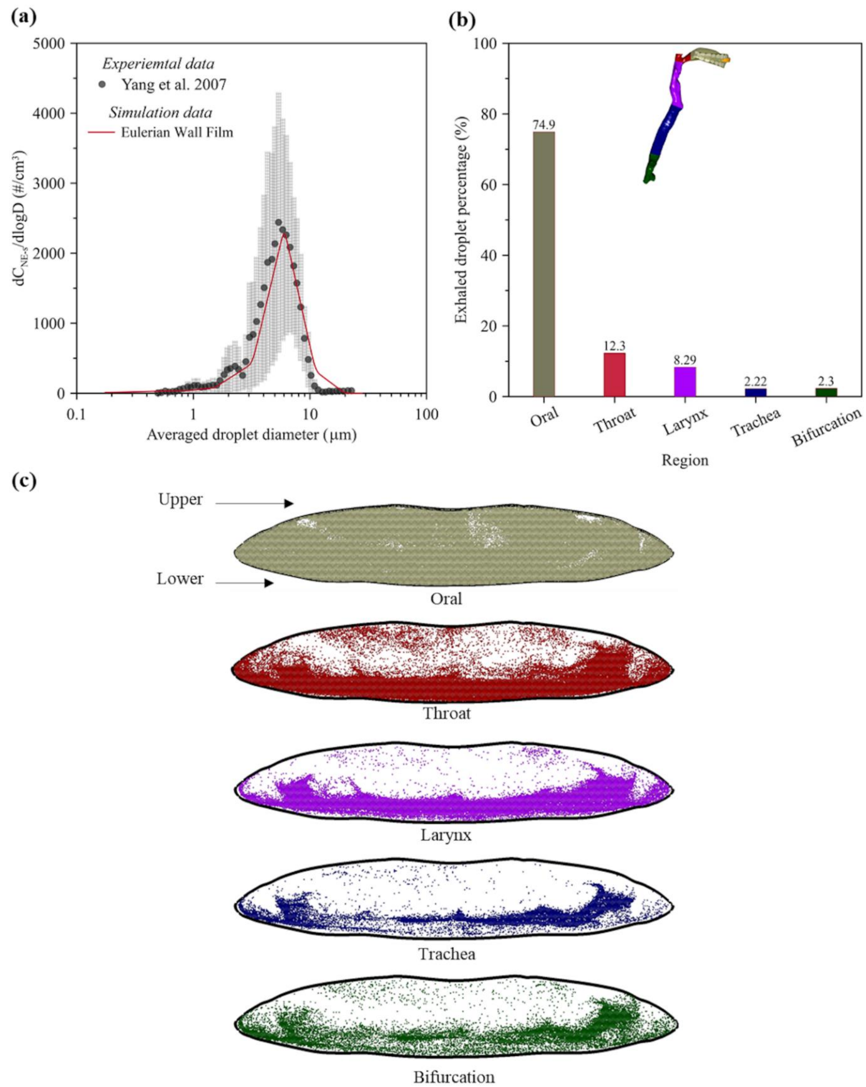

FIG. 6. (a) Validation of total concentration of exhaled droplets after one single cough event. (b) The percentage of exhaled droplets following their site origin. (c) Spatial distribution of exhaled droplets on the mouth opening after a single coughing episode.

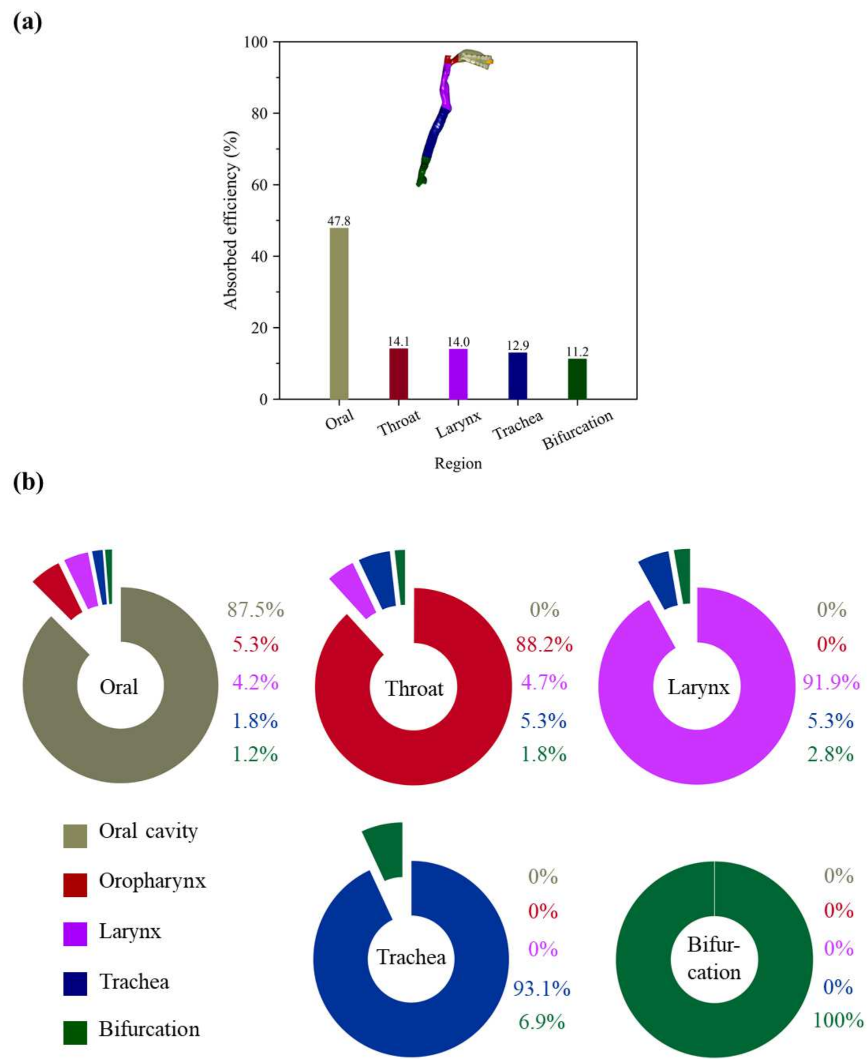

FIG. 7. (a) Total absorbed efficiency of the generated droplets on the inner surface of the airway region. (b) The absorption efficiency rate for different droplet source locations.

Accepted to Phys. Fluids 10.1063/5.0174014

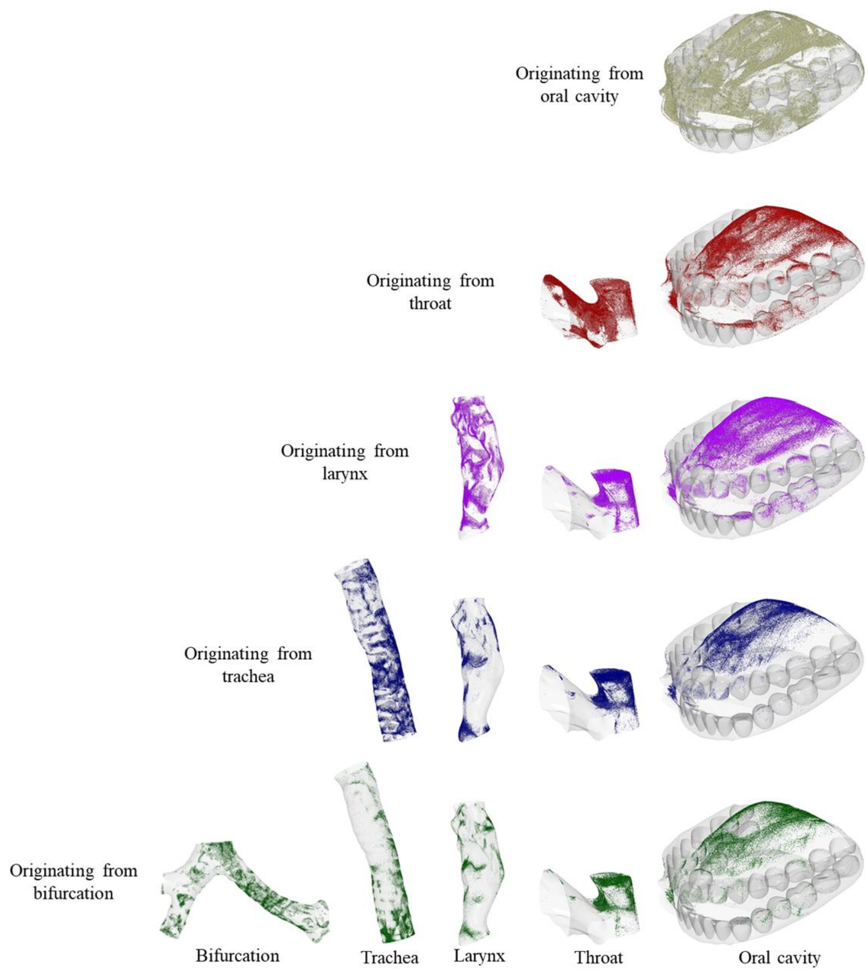

FIG. 8. Visualization of the absorbed droplets in local regions of the oral-tracheal model (column) derived from a specific location (row).

580

581

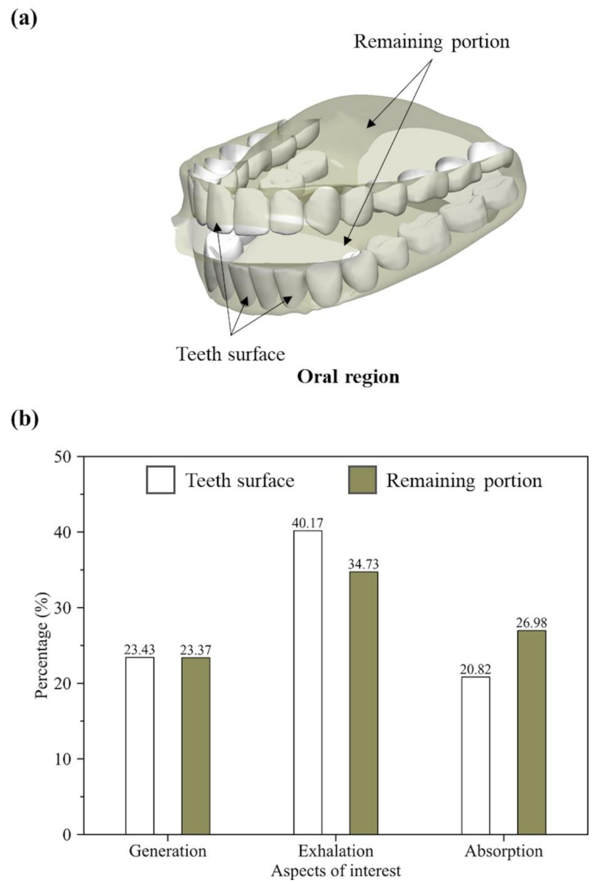

FIG. 9. (a) Outline of the oral cavity, including teeth surface and the remaining regions. (b)The total percentage of generation, exhalation, and absorption of droplets collapsed for the teeth surface and remaining portion.

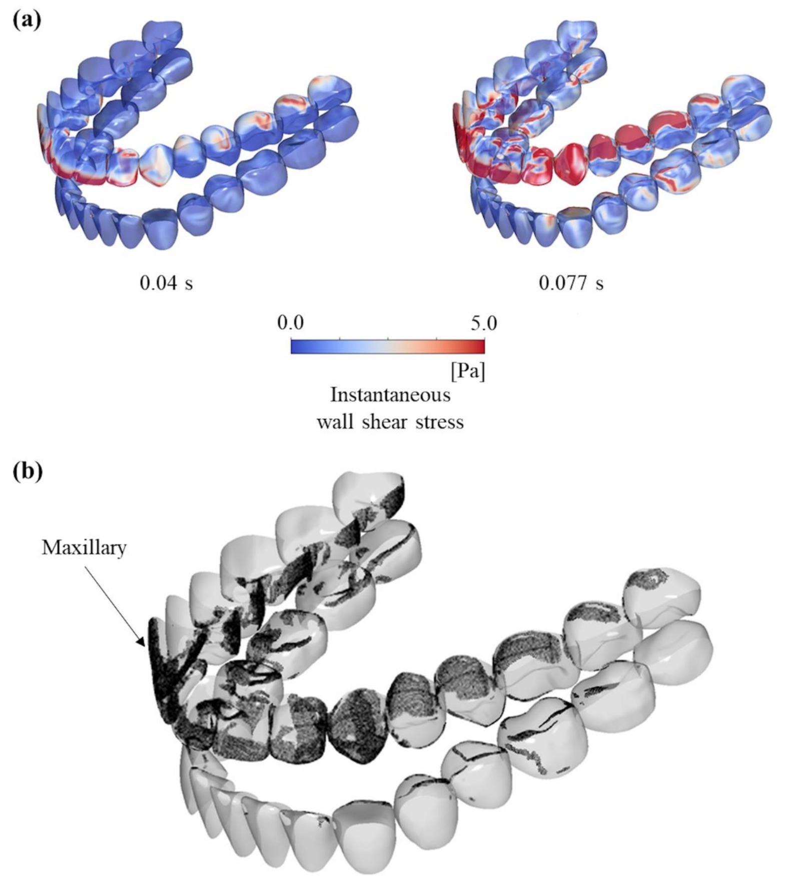

FIG. 10. (a) The instantaneous wall shear stress distribution on the teeth surface at 0.04 s (left) and 0.077 s (right). (b) Generated location and distribution of droplets on the teeth surface during coughing.

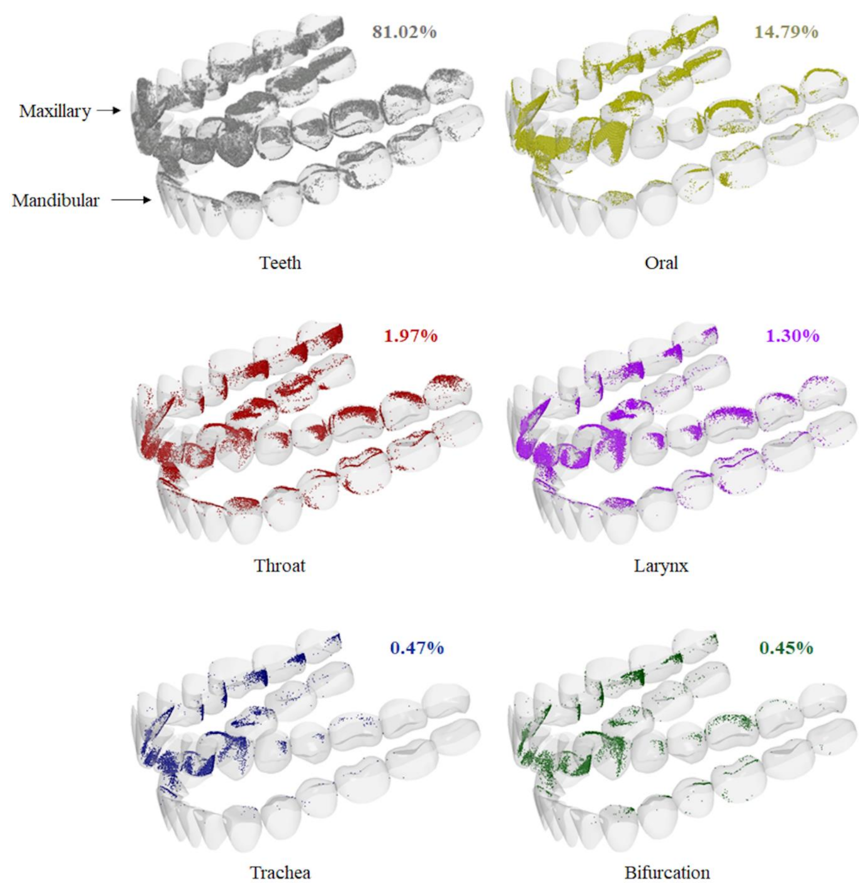

FIG. 11. 3D visualization of deposited droplets on the teeth surface colored by where the droplet was produced.

VII. TABLES

TABLE I. Numerical boundary conditions for the coughing airflow simulation.

Parameter	**Information**
Algorithm	SIMPLE (Semi-Implicit Method for Pressured Linked Equations
Convection scheme	Second order upwind
Density (kg/m^3)	1.185
Viscosity (kg/m s)	1.81x10^{-5}
Averaged cough peak flow rate (L/s)	5.75
Averaged cough exhaled volume (cm^3)	1,000
Total simulation time (s)	0.5
Time step size (s)	0.001

TABLE II. Initial parameter for Eulerian Wall film model.

Parameter	**Value**
Critical shear stress – CSS (Pa)	5
Diameter coefficient	0.0003
Mass coefficient	0.25
Surface tension (N/m)	0.0589

TABLE III. Classification of droplet size bin.

Droplet size bin (μm)	**Averaged size (μm)**
0.1 – 0.25	0.175
0.25 – 0.5	0.375
0.5 – 0.75	0.625
0.75 – 1.0	0.875
1.0 – 2.0	1.5
2.0 – 4.0	3.0
4.0 – 8.0	6.0
8.0 – 16.0	12.0
16.0 – 24.0	20.0
24.0 – 32.0	28.0

TABLE IV. Generated, exhaled, and absorbed efficiency of droplets during the coughing event following the droplet size bin.

Droplet size bin(μm)	**Generated percentage-$\eta_{G\text{-}s}$ [a] (%)**	**Exhaled percentage-$\eta_{E\text{-}s}$ [b] (%)**	**Absorbed percentage-$\eta_{A\text{-}s}$ [c] (%)**
0.1 – 0.25	0.078	0.49	0.044
0.25 – 0.5	0.133	0.79	0.078
0.5 – 0.75	0.149	0.65	0.108
0.75 – 1.0	0.181	0.50	0.157
1.0 – 2.0	1.94	2.60	1.94
2.0 – 4.0	11.81	12.82	11.58
4.0 – 8.0	78.01	73.06	78.47
8.0 – 16.0	7.53	8.93	7.47
16.0 – 24.0	0.15	0.15	0.15
24.0 – 32.0	0.019	0.01	0.003
Total percentage	100	100	100
Total number count	11,594,566 (N_G)	938,206 (N_E)	10,128,559 (N_A)

*[a,b,c] The percentage was calculated using Equations 15, 16 and 17

VIII. SUPPLEMENTARY MATERIAL

The supplementary material contains details and discussions regarding the optimization processes for the total mesh counts and the initial parameters for the EWF model, such as critical shear stress – *CSS* and diameter coefficient – *F*. In addition, detailed boundary conditions and results, which serve to reinforce the reliability of employing the EWF model to simulate the interaction between the free-stream flow and the lining fluid on the surface, are provided.

IX. LIMITATIONS

This study focused on a specific oral-tracheal model, which did not cover the individual-related variability. Besides, it is notable that the initial parameters for the EWF model including critical shear stress – *CSS* and diameter coefficient – *F* were emphasized by the individual structure and numerical boundary conditions of this study. In addition, a rigid airway model was assumed, which is the opposite of the elastic nature of the respiratory tract and ignores glottis deformation during coughing.

ACKNOWLEDGMENTS

This study was partially funded by Japan Science and Technology (JST), CREST Japan (JP 20356547), FOREST program from JST, Japan (JPMJFR225R) and JSPS KAKENHI (JP 22H00237, JP 22K18300, JP 20KK0099, JP 22K14371), and MEXT as "Program for Promoting Researches on the Supercomputer Fugaku" (JPMXP1020210316).

REFERENCES

Alexander-Brett, J., & Holtzman, M. J. (2015). Virus Infection of Airway Epithelial Cells. In *Mucosal Immunology* (pp. 1013–1021). Elsevier. https://doi.org/10.1016/B978-0-12-415847-4.00053-7

Aljabair, S., Alesbe, I., & Alkhalaf, A. (2023). CFD modeling of influenza virus diffusion during coughing and breathing in a ventilated room. *Journal of Thermal Engineering*, 127–137. https://doi.org/10.18186/thermal.1243491

Ansys® Academic Fluent, Release 2022 R2, Theory Guide, Eulerian Wall Films, ANSYS, Inc.

Anzai, H., Shindo, Y., Kohata, Y., Hasegawa, M., Takana, H., Matsunaga, T., Akaike, T., & Ohta, M. (2022). Coupled discrete phase model and Eulerian wall film model for numerical simulation of respiratory droplet generation during coughing. *Scientific Reports*, *12*(1), 14849. https://doi.org/10.1038/s41598-022-18788-3

Archer, J., McCarthy, L. P., Symons, H. E., Watson, N. A., Orton, C. M., Browne, W. J., Harrison, J., Moseley, B., Philip, K. E. J., Calder, J. D., Shah, P. L., Bzdek, B. R., Costello, D., & Reid, J. P. (2022). Comparing aerosol number and mass exhalation rates from children and adults during breathing, speaking and singing. *Interface Focus*, *12*(2), 20210078. https://doi.org/10.1098/rsfs.2021.0078

Assy, Z., Jager, D. H. J., Brand, H. S., & Bikker, F. J. (2022). Salivary film thickness and MUC5B levels at various intra-oral surfaces. *Clinical Oral Investigations*, *27*(2), 859–869. https://doi.org/10.1007/s00784-022-04626-3

Bahramian, A. (2023). Influence of indoor environmental conditions on airborne transmission and lifetime of sneeze droplets in a confined space: A way to reduce COVID-19 spread. *Environmental Science and Pollution Research*, *30*(15), 44067–44085. https://doi.org/10.1007/s11356-023-25421-x

Bahramian, A., & Ahmadi, G. (2023). Effect of sneeze flow velocity profiles on the respiratory droplets dispersion in a confined space: An experimental and computational fluid dynamics study. *Physics of Fluids*, *35*(6), 063330. https://doi.org/10.1063/5.0151254

Bourouiba, L. (2021). The Fluid Dynamics of Disease Transmission. *Annual Review of Fluid Mechanics*, *53*(1), 473–508. https://doi.org/10.1146/annurev-fluid-060220-113712

Bourouiba, L., Dehandschoewercker, E., & Bush, J. W. M. (2014). Violent expiratory events: On coughing and sneezing. *Journal of Fluid Mechanics*, *745*, 537–563. https://doi.org/10.1017/jfm.2014.88

Calmet, H., Inthavong, K., Both, A., Surapaneni, A., Mira, D., Egukitza, B., & Houzeaux, G. (2021). Large eddy simulation of cough jet dynamics, droplet transport, and inhalability over a ten minute exposure. *Physics of Fluids*, *33*(12), 125122. https://doi.org/10.1063/5.0072148

Chao, C. Y. H., Wan, M. P., Morawska, L., Johnson, G. R., Ristovski, Z. D., Hargreaves, M., Mengersen, K., Corbett, S., Li, Y., Xie, X., & Katoshevski, D. (2009). Characterization of expiration air jets and droplet size distributions immediately at the mouth opening. *Journal of Aerosol Science*, *40*(2), 122–133. https://doi.org/10.1016/j.jaerosci.2008.10.003

Churchyard, G., Kim, P., Shah, N. S., Rustomjee, R., Gandhi, N., Mathema, B., Dowdy, D., Kasmar, A., & Cardenas, V. (2017). What We Know About Tuberculosis Transmission: An Overview. *The Journal of Infectious Diseases*, *216*(suppl_6), S629–S635. https://doi.org/10.1093/infdis/jix362

Collins, L. M. C., & Dawes, C. (1987). The Surface Area of the Adult Human Mouth and Thickness of the Salivary Film Covering the Teeth and Oral Mucosa. *Journal of Dental Research*, *66*(8), 1300–1302. https://doi.org/10.1177/00220345870660080201

Dbouk, T., & Drikakis, D. (2020). On coughing and airborne droplet transmission to humans. *Physics of Fluids*, *32*(5), 053310. https://doi.org/10.1063/5.0011960

Dhand, R., & Li, J. (2020). Coughs and Sneezes: Their Role in Transmission of Respiratory Viral Infections, Including SARS-CoV-2. *American Journal of Respiratory and Critical Care Medicine*, *202*(5), 651–659. https://doi.org/10.1164/rccm.202004-1263PP

Elcner, J., Lizal, F., Jedelsky, J., Jicha, M., & Chovancova, M. (2016). Numerical investigation of inspiratory airflow in a realistic model of the human tracheobronchial airways and a comparison with experimental results. *Biomechanics and Modeling in Mechanobiology*, *15*(2), 447–469. https://doi.org/10.1007/s10237-015-0701-1

Gralton, J., Tovey, E. R., McLaws, M.-L., & Rawlinson, W. D. (2013). Respiratory virus RNA is detectable in airborne and droplet particles: Viral RNA in Airborne and Droplet Particles. *Journal of Medical Virology*, *85*(12), 2151–2159. https://doi.org/10.1002/jmv.23698

Guo, Y., Wei, J., Ou, C., Liu, L., Sadrizadeh, S., Jin, T., Tang, L., Zhang, Y., & Li, Y. (2020). Deposition of droplets from the trachea or bronchus in the respiratory tract during exhalation: A steady-state numerical investigation. *Aerosol Science and Technology*, *54*(8), 869–879. https://doi.org/10.1080/02786826.2020.1772459

Gupta, J. K., Lin, C.-H., & Chen, Q. (2009). Flow dynamics and characterization of a cough: Flow dynamics and characterization of a cough. *Indoor Air*, *19*(6), 517–525. https://doi.org/10.1111/j.1600-0668.2009.00619.x

Han, M., Ooka, R., Kikumoto, H., Oh, W., Bu, Y., & Hu, S. (2021). Measurements of exhaled airflow velocity through human coughs using particle image velocimetry. *Building and Environment*, *202*, 108020. https://doi.org/10.1016/j.buildenv.2021.108020

Harrison, J., Saccente-Kennedy, B., Orton, C. M., McCarthy, L. P., Archer, J., Symons, H. E., Szczepanska, A., Watson, N. A., Browne, W. J., Moseley, B., Philip, K. E. J., Hull, J. H., Calder, J. D., Costello, D., Shah, P. L., Epstein, R., Reid, J. P., & Bzdek, B. R. (2023). Emission rates, size distributions, and generation mechanism of oral respiratory droplets. *Aerosol Science and Technology*, 1–13. https://doi.org/10.1080/02786826.2022.2158778

Hegland, K. W., Troche, M. S., & Davenport, P. W. (2013). Cough expired volume and airflow rates during sequential induced cough. *Frontiers in Physiology*, *4*. https://doi.org/10.3389/fphys.2013.00167

Hossain, M., Chinenye-Kanu, N., Faisal, N. H., Prathuru, A., Asim, T., & Banik, S. (2023). Numerical Prediction of the Effect of Thermal Plume of a Standing Human on the Airborne Aerosol Flow in a Room: Assessment of the Social Distancing Rule. *Aerosol Science and Engineering*, *7*(1), 96–106. https://doi.org/10.1007/s41810-022-00165-2

Huang, N., Pérez, P., Kato, T., Mikami, Y., Okuda, K., Gilmore, R. C., Conde, C. D., Gasmi, B., Stein, S., Beach, M., Pelayo, E., Maldonado, J. O., Lafont, B. A., Jang, S.-I., Nasir, N., Padilla, R. J., Murrah, V. A., Maile, R., Lovell, W., … Byrd, K. M. (2021). SARS-CoV-2 infection of the oral cavity and saliva. *Nature Medicine*, *27*(5), 892–903. https://doi.org/10.1038/s41591-021-01296-8

Inthavong, K. (2020). From indoor exposure to inhaled particle deposition: A multiphase journey of inhaled particles. *Experimental and Computational Multiphase Flow*, *2*(2), 59–78. https://doi.org/10.1007/s42757-019-0046-6

Ito, K. (2016). Toward the development of an *in silico* human model for indoor environmental design. *Proceedings of the Japan Academy, Series B*, *92*(7), 185–203. https://doi.org/10.2183/pjab.92.185

Jayaweera, M., Perera, H., Gunawardana, B., & Manatunge, J. (2020). Transmission of COVID-19 virus by droplets and aerosols: A critical review on the unresolved dichotomy. *Environmental Research*, *188*, 109819. https://doi.org/10.1016/j.envres.2020.109819

Johnson, G. R., Morawska, L., Ristovski, Z. D., Hargreaves, M., Mengersen, K., Chao, C. Y. H., Wan, M. P., Li, Y., Xie, X., Katoshevski, D., & Corbett, S. (2011). Modality of human expired aerosol size distributions. *Journal of Aerosol Science*, *42*(12), 839–851. https://doi.org/10.1016/j.jaerosci.2011.07.009

Jones, R. M., & Brosseau, L. M. (2015). Aerosol Transmission of Infectious Disease. *Journal of Occupational & Environmental Medicine*, *57*(5), 501–508. https://doi.org/10.1097/JOM.0000000000000448

Kakimpa, B., Morvan, H. P., & Hibberd, S. (2015). Solution Strategies for Thin Film Rimming Flow Modelling. *Volume 5C: Heat Transfer*, V05CT15A026. https://doi.org/10.1115/GT2015-43503

Khoa, N. D., Li, S., Phuong, N. L., Kuga, K., Yabuuchi, H., Kan-O, K., Matsumoto, K., & Ito, K. (2023). Computational fluid-particle dynamics modeling of ultrafine to coarse particles deposition in the human respiratory system, down to the terminal bronchiole. *Computer Methods and Programs in Biomedicine*, *237*, 107589.

https://doi.org/10.1016/j.cmpb.2023.107589

Khoa, N. D., Phuong, N. L., Tani, K., Inthavong, K., & Ito, K. (2023). In-silico decongested trial effects on the impaired breathing function of a bulldog suffering from severe brachycephalic obstructive airway syndrome. *Computer Methods and Programs in Biomedicine*, *228*, 107243. https://doi.org/10.1016/j.cmpb.2022.107243

Kou, G., Li, X., Wang, Y., Lin, M., Zeng, Y., Yang, X., Yang, Y., & Gan, Z. (2018). CFD Simulation of Airflow Dynamics During Cough Based on CT-Scanned Respiratory Airway Geometries. *Symmetry*, *10*(11), 595. https://doi.org/10.3390/sym10110595

Kuga, K., Ito, K., Chen, W., Wang, P., Fowles, J., & Kumagai, K. (2021). Secondary indoor air pollution and passive smoking associated with cannabis smoking using electric cigarette device–demonstrative in silico study. *PLOS Computational Biology*, *17*(5), e1009004. https://doi.org/10.1371/journal.pcbi.1009004

Kuga, K., Kizuka, R., Khoa, N. D., & Ito, K. (2023). Effect of transient breathing cycle on the depositionÂ of micro and nanoparticles on respiratory walls. *Computer Methods and Programs in Biomedicine*, *236*, 107501. https://doi.org/10.1016/j.cmpb.2023.107501

Kuga, K., Sakamoto, M., Wargocki, P., & Ito, K. (2022). Prediction of exhaled carbon dioxide concentration using a computer-simulated person that included alveolar gas exchange. *Indoor Air*, *32*(8).

Li, A., & Ahmadi, G. (1992). Dispersion and Deposition of Spherical Particles from Point Sources in a Turbulent Channel Flow. *Aerosol Science and Technology*, *16*(4), 209–226. https://doi.org/10.1080/02786829208959550

Li, H., Kuga, K., & Ito, K. (2022). SARS-CoV-2 Dynamics in the Mucus Layer of the Human Upper Respiratory Tract Based on Host–Cell Dynamics. *Sustainability*, *14*(7), 3896. https://doi.org/10.3390/su14073896

Li, H., Leong, F. Y., Xu, G., Kang, C. W., Lim, K. H., Tan, B. H., & Loo, C. M. (2021). Airborne dispersion of droplets during coughing: A physical model of viral transmission. *Scientific Reports*, *11*(1), 4617. https://doi.org/10.1038/s41598-021-84245-2

Li, X., Mak, C. M., Ai, Z., Ma, K. W., & Wong, H. M. (2023). Numerical investigation of the impacts of environmental conditions and breathing rate on droplet transmission during dental service. *Physics of Fluids*, *35*(4), 043332. https://doi.org/10.1063/5.0144647

Lindsley, W. G., Pearce, T. A., Hudnall, J. B., Davis, K. A., Davis, S. M., Fisher, M. A., Khakoo, R., Palmer, J. E., Clark, K. E., Celik, I., Coffey, C. C., Blachere, F. M., & Beezhold, D. H. (2012). Quantity and Size Distribution of Cough-Generated Aerosol Particles Produced by Influenza Patients During and After Illness. *Journal of Occupational and Environmental Hygiene*, *9*(7), 443–449. https://doi.org/10.1080/15459624.2012.684582

Mariam, Magar, A., Joshi, M., Rajagopal, P. S., Khan, A., Rao, M. M., & Sapra, B. K. (2021). CFD Simulation of the Airborne Transmission of COVID-19 Vectors Emitted during

Respiratory Mechanisms: Revisiting the Concept of Safe Distance. *ACS Omega*, *6*(26), 16876–16889. https://doi.org/10.1021/acsomega.1c01489

Morawska, L. (2006). Droplet fate in indoor environments, or can we prevent the spread of infection? *Indoor Air*, *16*(5), 335–347. https://doi.org/10.1111/j.1600-0668.2006.00432.x

Morawska, L., Johnson, G. R., Ristovski, Z. D., Hargreaves, M., Mengersen, K., Corbett, S., Chao, C. Y. H., Li, Y., & Katoshevski, D. (2009). Size distribution and sites of origin of droplets expelled from the human respiratory tract during expiratory activities. *Journal of Aerosol Science*, *40*(3), 256–269. https://doi.org/10.1016/j.jaerosci.2008.11.002

Murga, A., Bale, R., Li, C.-G., Ito, K., & Tsubokura, M. (2023). Large eddy simulation of droplet transport and deposition in the human respiratory tract to evaluate inhalation risk. *PLOS Computational Biology*, *19*(3), e1010972. https://doi.org/10.1371/journal.pcbi.1010972

Nie, Z., Chen, Y., & Deng, M. (2022). Quantitative evaluation of precautions against the COVID-19 indoor transmission through human coughing. *Scientific Reports*, *12*(1), 22573. https://doi.org/10.1038/s41598-022-26837-0

Nishandar, S. R., He, Y., Princevac, M., & Edwards, R. D. (2023). Fate of Exhaled Droplets From Breathing and Coughing in Supermarket Checkouts and Passenger Cars. *Environmental Health Insights*, *17*, 117863022211482. https://doi.org/10.1177/11786302221148274

Pairetti, C., Villiers, R., & Zaleski, S. (2021). On shear layer atomization within closed channels: Numerical simulations of a cough-replicating experiment. *Computers & Fluids*, *231*, 105125. https://doi.org/10.1016/j.compfluid.2021.105125

Payri, R., Martí-Aldaraví, P., Quintero, P. M., & Marco-Gimeno, J. (2021). LARGE EDDY SIMULATION FOR THE PREDICTION OF HUMAN COUGHING. *Atomization and Sprays*, *31*(9), 49–73. https://doi.org/10.1615/AtomizSpr.2021037129

Paz, C., Suárez, E., Parga, O., & Vence, J. (2017). Glottis effects on the cough clearance process simulated with a CFD dynamic mesh and Eulerian wall film model. *Computer Methods in Biomechanics and Biomedical Engineering*, *20*(12), 1326–1338. https://doi.org/10.1080/10255842.2017.1360872

Paz, C., Suárez, E., & Vence, J. (2017). CFD transient simulation of the cough clearance process using an Eulerian wall film model. *Computer Methods in Biomechanics and Biomedical Engineering*, *20*(2), 142–152. https://doi.org/10.1080/10255842.2016.1206532

Paz, C., Suárez, E., Vence, J., & Cabarcos, A. (2019). Analysis of the volume of fluid (VOF) method for the simulation of the mucus clearance process with CFD. *Computer Methods in Biomechanics and Biomedical Engineering*, *22*(5), 547–566. https://doi.org/10.1080/10255842.2019.1569637

Phuong, N. L., & Ito, K. (2015). Investigation of flow pattern in upper human airway including oral and nasal inhalation by PIV and CFD. *Building and Environment*, *94*, 504–515. https://doi.org/10.1016/j.buildenv.2015.10.002

Piret, J., & Boivin, G. (2021). Pandemics Throughout History. *Frontiers in Microbiology*, *11*, 631736. https://doi.org/10.3389/fmicb.2020.631736

Pöhlker, M. L., Krüger, O. O., Förster, J.-D., Berkemeier, T., Elbert, W., Fröhlich-Nowoisky, J., Pöschl, U., Pöhlker, C., Bagheri, G., Bodenschatz, E., Huffman, J. A., Scheithauer, S., & Mikhailov, E. (2021). *Respiratory aerosols and droplets in the transmission of infectious diseases* (arXiv:2103.01188). arXiv. http://arxiv.org/abs/2103.01188

Rajendran, R. R., & Banerjee, A. (2019). Mucus transport and distribution by steady expiration in an idealized airway geometry. *Medical Engineering & Physics*, *66*, 26–39. https://doi.org/10.1016/j.medengphy.2019.02.006

Ren, S., Cai, M., Shi, Y., Luo, Z., & Wang, T. (2022). Influence of cough airflow characteristics on respiratory mucus clearance. *Physics of Fluids*, *34*(4), 041911. https://doi.org/10.1063/5.0088100

Ren, S., Li, W., Wang, L., Shi, Y., Cai, M., Hao, L., Luo, Z., Niu, J., Xu, W., & Luo, Z. (2020). Numerical Analysis of Airway Mucus Clearance Effectiveness Using Assisted Coughing Techniques. *Scientific Reports*, *10*. https://doi.org/10.1038/s41598-020-58922-7

Ren, S., Shi, Y., Cai, M., Zhao, H., & Zhang, Z. (2018). ANSYS-MATLAB co-simulation of mucus flow distribution and clearance effectiveness of a new simulated cough device. *International Journal for Numerical Methods in Biomedical Engineering*, *34*(6). https://doi.org/10.1002/cnm.2978

Saffman, P. G. (1965). The lift on a small sphere in a slow shear flow. *Journal of Fluid Mechanics*, *22*(2), 385–400. https://doi.org/10.1017/S0022112065000824

Schaefer, A., & Lai, S. K. (2022). The biophysical principles underpinning muco-trapping functions of antibodies. *Human Vaccines & Immunotherapeutics*, *18*(2), 1939605. https://doi.org/10.1080/21645515.2021.1939605

Seminara, G., Carli, B., Forni, G., Fuzzi, S., Mazzino, A., & Rinaldo, A. (2020). Biological fluid dynamics of airborne COVID-19 infection. *Rendiconti Lincei. Scienze Fisiche e Naturali*, *31*(3), 505–537. https://doi.org/10.1007/s12210-020-00938-2

SeyedAlinaghi, S., Karimi, A., Mojdeganlou, H., Pashaei, Z., Mirzapour, P., Shamsabadi, A., Barzegary, A., Afroughi, F., Dehghani, S., Janfaza, N., Fakhfouri, A., Khodaei, S., Mehraeen, E., & Dadras, O. (2022). Minimum infective dose of severe acute respiratory syndrome coronavirus 2 based on the current evidence: A systematic review. *SAGE Open Medicine*, *10*, 205031212211150. https://doi.org/10.1177/20503121221115053

Shelley, D. A., Sih, B. L., & Ng, L. J. (2014). *An integrated physiology model to study regional lung damage effects and the physiologic response*. 19.

Sosnowski, T. R. (2021). Inhaled aerosols: Their role in COVID-19 transmission, including biophysical interactions in the lungs. *Current Opinion in Colloid & Interface Science*, *54*, 101451. https://doi.org/10.1016/j.cocis.2021.101451

Stadnytskyi, V., Anfinrud, P., & Bax, A. (2021). Breathing, speaking, coughing or sneezing: What drives transmission of SARS-CoV-2? *Journal of Internal Medicine*, *290*(5), 1010–1027. https://doi.org/10.1111/joim.13326

To, K. K.-W., Tsang, O. T.-Y., Yip, C. C.-Y., Chan, K.-H., Wu, T.-C., Chan, J. M.-C., Leung, W.-S., Chik, T. S.-H., Choi, C. Y.-C., Kandamby, D. H., Lung, D. C., Tam, A. R., Poon, R. W.-S., Fung, A. Y.-F., Hung, I. F.-N., Cheng, V. C.-C., Chan, J. F.-W., & Yuen, K.-Y. (2020). Consistent Detection of 2019 Novel Coronavirus in Saliva. *Clinical Infectious Diseases*, *71*(15), 841–843. https://doi.org/10.1093/cid/ciaa149

Wang, C. C., Prather, K. A., Sznitman, J., Jimenez, J. L., Lakdawala, S. S., Tufekci, Z., & Marr, L. C. (2021). Airborne transmission of respiratory viruses. *Science*, *373*(6558), eabd9149. https://doi.org/10.1126/science.abd9149

Wang, C., Yoo, S.-J., Tanabe, S., & Ito, K. (2020). Investigation of transient and heterogeneous micro-climate around a human body in an enclosed personalized work environment. *Energy and Built Environment*, *1*(4), 423–431. https://doi.org/10.1016/j.enbenv.2020.04.011

Wang, H., Li, Z., Zhang, X., Zhu, L., Liu, Y., & Wang, S. (2020). The motion of respiratory droplets produced by coughing. *Physics of Fluids*, *32*(12), 125102. https://doi.org/10.1063/5.0033849

Wei, J., & Li, Y. (2016). Airborne spread of infectious agents in the indoor environment. *American Journal of Infection Control*, *44*(9), S102–S108. https://doi.org/10.1016/j.ajic.2016.06.003

Widders, A., Broom, A., & Broom, J. (2020). SARS-CoV-2: The viral shedding vs infectivity dilemma. *Infection, Disease & Health*, *25*(3), 210–215. https://doi.org/10.1016/j.idh.2020.05.002

Wölfel, R., Corman, V. M., Guggemos, W., Seilmaier, M., Zange, S., Müller, M. A., Niemeyer, D., Jones, T. C., Vollmar, P., Rothe, C., Hoelscher, M., Bleicker, T., Brünink, S., Schneider, J., Ehmann, R., Zwirglmaier, K., Drosten, C., & Wendtner, C. (2020). Virological assessment of hospitalized patients with COVID-2019. *Nature*, *581*(7809), 465–469. https://doi.org/10.1038/s41586-020-2196-x

Wyllie, A. L., Fournier, J., Casanovas-Massana, A., Campbell, M., Tokuyama, M., Vijayakumar, P., Warren, J. L., Geng, B., Muenker, M. C., Moore, A. J., Vogels, C. B. F., Petrone, M. E., Ott, I. M., Lu, P., Venkataraman, A., Lu-Culligan, A., Klein, J., Earnest, R., Simonov, M., … Ko, A. I. (2020). Saliva or Nasopharyngeal Swab Specimens for Detection of SARS-CoV-2. *New England Journal of Medicine*, *383*(13), 1283–1286. https://doi.org/10.1056/NEJMc2016359

Yan, J., Grantham, M., Pantelic, J., Bueno De Mesquita, P. J., Albert, B., Liu, F., Ehrman, S., Milton, D. K., EMIT Consortium, Adamson, W., Beato-Arribas, B., Bischoff, W., Booth, W., Cauchemez, S., Ehrman, S., Enstone, J., Ferguson, N., Forni, J., Gilbert, A., … Tellier, R. (2018). Infectious virus in exhaled breath of symptomatic seasonal influenza cases from a college community. *Proceedings of the National Academy of Sciences*, *115*(5), 1081–1086. https://doi.org/10.1073/pnas.1716561115

Yang, S., Lee, G. W. M., Chen, C.-M., Wu, C.-C., & Yu, K.-P. (2007). The Size and Concentration of Droplets Generated by Coughing in Human Subjects. *Journal of Aerosol Medicine*, *20*(4), 484–494. https://doi.org/10.1089/jam.2007.0610

Yi, H., Wang, Q., & Feng, Y. (2021). Computational analysis of obstructive disease and cough intensity effects on the mucus transport and clearance in an idealized upper airway model using the volume of fluid method. *Physics of Fluids*, *33*(2), 021903. https://doi.org/10.1063/5.0037764

Yoo, S., & Ito, K. (2022). Validation, verification, and quality control of computational fluid dynamics analysis for indoor environments using a computer-simulated person with respiratory tract. *JAPAN ARCHITECTURAL REVIEW*, *5*(4), 714–727. https://doi.org/10.1002/2475-8876.12301

Zayas, G., Chiang, M. C., Wong, E., MacDonald, F., Lange, C. F., Senthilselvan, A., & King, M. (2012). Cough aerosol in healthy participants: Fundamental knowledge to optimize droplet-spread infectious respiratory disease management. *BMC Pulmonary Medicine*, *12*(1), 11. https://doi.org/10.1186/1471-2466-12-11

Zhou, M., & Zou, J. (2021). A dynamical overview of droplets in the transmission of respiratory infectious diseases. *Physics of Fluids*, *33*(3), 031301. https://doi.org/10.1063/5.0039487

Zore, K., Parkhi, G., Sasanapuri, B., & Varghese, A. (2019). 21th Annual CFD Symposium, August 8-9, 2019, Bangalore. *Annual CFD Symposium*, 0–11.

Zuo, Y. Y., Uspal, W. E., & Wei, T. (2020). Airborne Transmission of COVID-19: Aerosol Dispersion, Lung Deposition, and Virus-Receptor Interactions. *ACS Nano*, *14*(12), 16502–16524. https://doi.org/10.1021/acsnano.0c08484

CONFLICT OF INTEREST STATEMENT

The authors declare that they have no competing financial interests or personal relationships that could have influenced the work reported in this paper.

DATA AVAILABILITY

The data supporting this study's findings are available from the corresponding author upon reasonable request.